

# Nanoscale

Accepted Manuscript



This is an *Accepted Manuscript*, which has been through the Royal Society of Chemistry peer review process and has been accepted for publication.

*Accepted Manuscripts* are published online shortly after acceptance, before technical editing, formatting and proof reading. Using this free service, authors can make their results available to the community, in citable form, before we publish the edited article. We will replace this *Accepted Manuscript* with the edited and formatted *Advance Article* as soon as it is available.

You can find more information about *Accepted Manuscripts* in the [Information for Authors](#).

Please note that technical editing may introduce minor changes to the text and/or graphics, which may alter content. The journal's standard [Terms & Conditions](#) and the [Ethical guidelines](#) still apply. In no event shall the Royal Society of Chemistry be held responsible for any errors or omissions in this *Accepted Manuscript* or any consequences arising from the use of any information it contains.

## ARTICLE

## Defect related emission *versus* intersystem crossing: Blue emitting ZnO/graphene oxide quantum dots

Cite this: DOI: 10.1039/x0xx00000x

Sesha Vempati,\*<sup>a</sup> Asli Celebioglu and Tamer Uyar<sup>a,b</sup>Received 00th October 2013,  
Accepted 00th October 2013

DOI: 10.1039/x0xx00000x

www.rsc.org/

In Ref. [Nat. Nanotechnol. 2012, Vol 7, 465-471] interesting optoelectronic properties of ZnO/graphene oxide (GO) composite were presented. Essentially, in the luminescence spectrum indirect optical transitions were identified to be from epoxy group of GO ( $\text{GO}_{\text{epoxy}}$ ) to the valance band ( $E_v$ ) of ZnO. *Viz* 406 nm, L1:  $(\text{LUMO} + 2)_{\text{GO}_{\text{epoxy}}} \rightarrow E_v$  and 436 nm, L2:  $(\text{LUMO})_{\text{GO}_{\text{epoxy}}} \rightarrow E_v$ . Furthermore, the emission peaked at ~550 nm is attributed to zinc interstitials ( $\text{Zn}_i$ ) or oxygen vacancies ( $V_{\text{O}}$ ) and shown to span from 350-650 nm (equivalent to a width of ~0.8 eV). In this report we accentuate two vital though largely ignored concerns as itemized in the following. (i) By considering the growth mechanism of ZnO in the composite, there is a certain possibility that these two bands (L1 and L2) may be originated from intrinsic defects of ZnO such as  $\text{Zn}_i$ s and extended  $\text{Zn}_i$ s (ex- $\text{Zn}_i$ s). Or L1 and L2 might be intrinsic to GO. (ii) The 550 nm emission involves  $V_{\text{O}}$ s and consists of two components with a typical width of ~0.3 eV. Here we present the results of a thorough investigation confirming the presence of  $\text{Zn}_i$ s, ex- $\text{Zn}_i$ s and intrinsic emission from GO. We also note that during the synthesis the presence of dimethyl formamide significantly affected the emission from GO in addition to some chemical modifications. Apart from these, we have discussed other crucial factors which require deeper attention in the context of luminescence from complex systems such as the present.

### Introduction

In recent years graphene oxide (GO) has attracted a lot of research attention,<sup>1-9</sup> where its potential is self-standing in its pure form.<sup>2,6,10,11</sup> However, the properties can be enhanced/ tuned via combinations<sup>2,4,8,9,12-14</sup> especially for optical and optoelectronic applications.<sup>3-5,13</sup> In any case as a prerequisite a clear understanding of the emission properties is essential for future developments,<sup>2,4,5</sup> however, in which context the optical properties of GO are debated, where the fluorescence is attributed to the oxygen functional groups (C–O, C = O, and O–C=O) or to the localization of  $sp^2$  carbons.<sup>2,5</sup> While keeping that in mind, in the case of intercalating structure,<sup>2,4</sup> the intricacy of the optical properties is of course not abated, where an overlap of the emission bands is present. Nevertheless, we have recently deconvoluted in the case of a GO/polyaniline intercalating compound despite of an overlap of emission lines.<sup>4</sup> It is an undisputed fact that the composites of GO are potential<sup>2,3,8,9,13,15</sup> when combined with other materials such as ZnO,<sup>2,3</sup> TiO<sub>2</sub>,<sup>15</sup> etc. The emission properties are strongly dependent on the type of interaction between GO and the other constituent,<sup>2,4,14,15</sup> eg. intersystem crossings in TiO<sub>2</sub>/GO by Bao et al.<sup>15</sup> and ZnO/GO by Son et al.<sup>3</sup> Please refer to Ref.<sup>2</sup> for more examples and associated interactions. Among these, the case with ZnO is not only intriguing,<sup>3,16</sup> but also quite intertwined, especially when the fluorescence from GO superpose with the defect related emission of ZnO.<sup>2,16-23</sup> In conjunction with this, we turn our attention to the emission properties of ZnO/GO quantum dots (QDs), precisely to Ref.<sup>3</sup> While elucidating the emission properties of GO/ZnO QDs the observed blue emission bands were attributed to transitions L1:  $(\text{LUMO} + 2)_{\text{GO}_{\text{epoxy}}} \rightarrow E_v$  and L2:  $(\text{LUMO})_{\text{GO}_{\text{epoxy}}} \rightarrow E_v$ , where LUMO-lowest unoccupied molecular orbital,  $\text{GO}_{\text{epoxy}}$ -epoxy groups of GO and  $E_v$  is

the valance band of ZnO.<sup>3</sup> Besides, green emission is attributed to oxygen vacancies ( $V_{\text{O}}$ ) or zinc interstitials ( $\text{Zn}_i$ ).<sup>3</sup>

In this report we highlight that the emission wavelengths of  $\text{Zn}_i \rightarrow E_v$  and ex- $\text{Zn}_i \rightarrow E_v$  overlap with that of L1 and L2, respectively, where ex- $\text{Zn}_i$ -extended  $\text{Zn}_i$ s. Despite we do not rule out the earlier discussed transitions,<sup>3</sup> rather we report on evidences of defect related and others emissions which were largely ignored. Furthermore, the green emission in fact, is attributed to  $V_{\text{O}}$ s,<sup>16-23</sup> and consists of two components (bulk and depletion<sup>16,17,19,23</sup>) however not to the presence of  $\text{Zn}_i$ s. Since GO can be a *p*-type material (depending on the level of oxidation),<sup>6,10,11</sup> in the presence of ZnO it may form depletion region and influence the emission characteristics as noted here. Furthermore, this report provides a general though vital mapping of crucial factors in analyzing the heterocombinations such as graphene (oxide) and inorganic semiconductors.

### Experimental

All the starting materials were received from Sigma and used as received. GO,<sup>4,6,7</sup> ZnO QDs,<sup>3</sup> and ZnO/GO QDs,<sup>3</sup> were synthesized as described in the given references. Additionally to unveil the influence of dimethyl formamide (DMF) we have treated GO with it ( $\text{GO}_{\text{DMF}}$ ) at 95 °C for 5 h which matches the reaction condition of ZnO/GO QDs without zinc acetate. These ZnO/GO QDs and  $\text{GO}_{\text{DMF}}$  were subjected to repeated washing with ethanol through centrifugation and finally with deionized water. All the samples were dried at 45 °C overnight under vacuum. Samples were subjected to transmission electron microscopy (TEM, FEI-Tecnai G2 F30) when dispersed in ethanol or deionized water and analyzed from a Cu-grid (no holey carbon coating). TEM images were processed with ImageJ (version 1.42q) software for their fast Fourier transform (FFT) counterparts. X-ray diffraction patterns (XRD) were obtained from a

PANalytical X'pert Pro MPD ( $\lambda_{\text{Cu-K}\alpha} = 1.5418 \text{ \AA}$ ). The ionic state of elements at the surface of the samples was investigated by X-ray photoelectron spectroscopy (XPS, ThermoScientific K-Alpha,  $h\nu_{\text{Al-K}\alpha} = 1486.6 \text{ eV}$ ) with a flood-gun charge neutralizer. XPS peak deconvolution is performed with Avantage software. Raman spectroscopy was performed with WITec instruments (Alpha 300S, 532 nm laser). Emission responses were recorded from Horiba Scientific FL-1057 TCSPC at an excitation wavelength of  $\sim 350 \text{ nm}$ . Optical emission (Gaussian, standard deviation (SD)  $\sim 2\text{-}3 \text{ nm}$ ), Raman spectra (Lorentzian, SD  $\sim 2 \text{ cm}^{-1}$ ) and XRD (Lorentzian, SD  $\sim 0.003^\circ$ ) were deconvoluted with OriginPro 8.5. Apart from the number of peaks, the other parameters were set as free until convergence except the center of two components for the deconvolution of the green emission is fixed at 524 (C1) and 577 nm (C2) based on the knowledge from the literature.<sup>16,17,19,23</sup> Raman peak in fluorescence spectra is fixed at  $\sim 378 \text{ nm}$  for  $\text{GO}_{\text{DMF}}$ .

## Results and discussion

The ionic interaction between  $\text{Zn}^{2+}$  ions and the oxygen-containing functional groups ( $-\text{O}-$ ,  $-\text{OH}$  and  $-\text{COOH}$ ) of GO is schematized in Figure 1a-c, after Son et al.<sup>3</sup> The differences in the electronegativity/proton donating nature of these functional groups enable such interaction with cation. Based on this interaction it can be suggested that ZnO QDs growth is initiated on GO where the oxygenous functional groups are more dense. As a consequence it is expected that the ZnO QDs may be not entirely covered by GO. The effects of the uncovered ZnO are discussed in the emission properties. Contextually if the interaction between the adsorbate and substrate is much less than that of adsorbed molecules itself, then the influence of substrate on the superstructure can be ignored. In any case, the influence of the substrate on the superstructure will be evident in the structural investigation, e.g. XRD. Furthermore after the growth the final structure of ZnO QDs can host lattice defects, if radiative, can be identified in photoluminescence (PL). Note that the site specific localized lattice defects will be spatially integrated over the probe beam area (XPS:  $\sim 400 \mu\text{m}^2$ , optical emission:  $\sim 8 \text{ mm}^2$ , Raman:  $\sim 0.13 \mu\text{m}^2$ ).

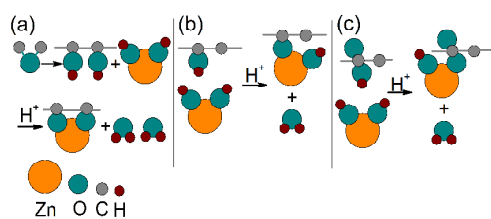


**Fig. 1.** Interaction between  $\text{Zn}^{2+}$  ion and (a) epoxy, (b) hydroxyl and (c) carboxyl groups of GO. Diagram not to scale.

Representative TEM images of GO, ZnO QDs and ZnO/GO QDs are shown along with the FFT on Figure 2. Probably single layer of graphene suggests successful exfoliation of graphite while its wrinkles or folds are consistent with the earlier reports.<sup>4,6,7</sup> The ZnO QD is shown as an inset of Figure 2a. The lattice spacing is found to be  $\sim 2.25 \text{ \AA}$ , corresponding to the  $c$ -axis. High resolution image from ZnO/GO QDs is shown in Figure 2b. There are regions annotated with 1 and 2 clearly show the honeycomb lattice of graphene. Earlier it is anticipated that ZnO QDs grow on graphene in which context we have selected two regions (3 & 4) for a closer inspection. In the first glance, region 3 is darker than 4 presumably due to the differences in the electron transparency either because of the differences in the properties of material and/or thickness. The FFT counterparts of regions 3 and 4 are shown on top of the

selection on Figure 2b. FFT of region 3 indicated two sets of intensities and one of which corresponds to GO (hexagonal shaped, red dots) while the other to ZnO (blue dots). While the FFT of region 4 depicted pattern from ZnO lattice while that of GO is not seen at an identifiable intensity level. Nevertheless, the presence of graphene is not denied in region 4, perhaps it might be not in the focus due to possible wrinkles and/or folds. This analysis suggests that the ZnO QDs are in fact grown on GO sheets.

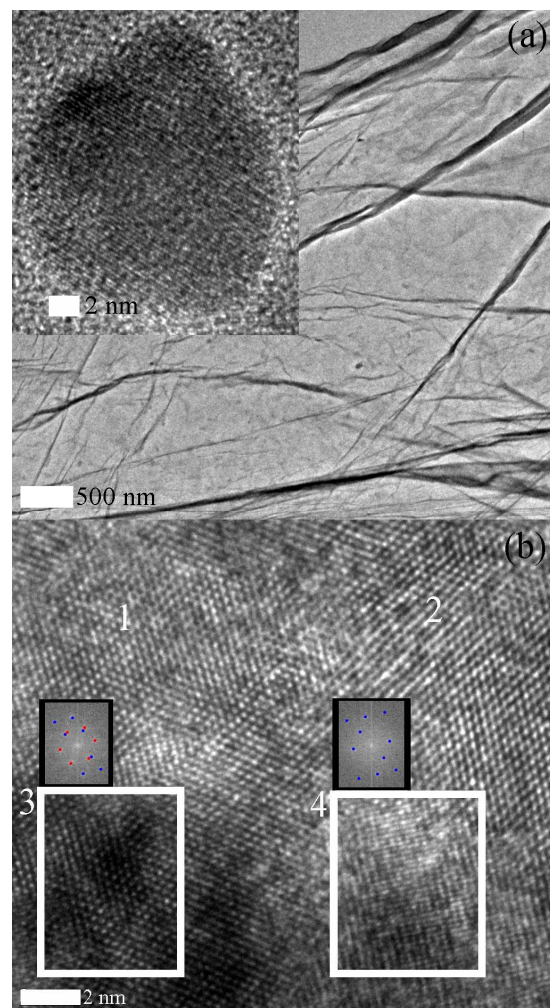


**Fig. 2.** TEM images of (a) GO, insert shows a ZnO QD (b) atomic resolved ZnO/GO QD, where FFT image of the boxed region (white) is shown. Red and blue spots correspond to graphene and ZnO lattices respectively.

XRD-patterns from various samples are shown in Figure 3 where the corresponding reflections were identified. GO has shown a single reflection depicting an interplanar spacing ( $d_{\text{GO}}$ ) of  $\sim 8.379 \text{ \AA}$  which is consistent with the literature *vis-a-vis*  $d_{\text{graphite}} \approx 3.368 \text{ \AA}$ .<sup>6,7</sup> After oxidation the oxygenous functional groups increase the distance between the graphene sheets which were stacked otherwise under the influence of van der Waal's force. Pattern from  $\text{GO}_{\text{DMF}}$  has sustained the (002) reflection, however, close inspection of this peak (Figure 3b) suggests a shift to higher Bragg's angle than that of GO. It appears to be the case that the DMF treatment reduced some of the functional groups bringing the graphene sheets closer ( $d_{\text{GO}_{\text{DMF}}} = \sim 7.968 \text{ \AA}$ ). The consequence of lowered degree of oxidation may be reflected in fluorescence<sup>2</sup> and Raman spectroscopies. Pattern from

ZnO QDs suggests a polycrystalline wurtzite structure and matches with the literature (Figure 3a).<sup>3,16,17,23</sup> Furthermore (100), (002) and (101) reflections from ZnO containing samples in Figure 3c. A clear angular shift for ZnO/GO QDs to higher  $2\theta$  values results from the developed strain. A closer inspection of the full width at half maximum (fwhm) values of ZnO QDs and ZnO/GO QDs suggests sharper peaks for the former, in other words higher crystallite size. Furthermore, the peaks from ZnO/GO QDs did not appear to have shoulders at lower  $2\theta$  values which rules out the existence of uncovered ZnO QDs within the detection limits of XRD. This is convincing by given the fact that  $Zn^{2+}$  ions are hoisted by the oxygenous functional groups and the QD growth takes place on the surface of the GO sheets which is corroborated by the TEM investigations. As speculated in the growth model, the 'substrate (GO) effect' is reflected in the angular shift of diffraction peaks. In the case of QDs there is no much of 'bulk' formed due to their zero dimension.<sup>24</sup> The absence of bulk material in fact poses dramatic effect on its properties as the shift of  $2\theta$  corresponds to the whole material (high penetration depth of the probe X-rays<sup>25</sup>). In the case of the induced stress additional effects can be expected on optoelectronic properties in general.<sup>26-28</sup> Vacancies or other defects may be formed to relieve the interfacial strain.<sup>29</sup> Typically the surface stress ( $\sim 1$  N/m) is confined to a distance of 1 nm from the surface.<sup>29</sup> Nevertheless, in the course of ZnO/GO QDs synthesis, the possibility of formation of defects such as  $V_{OS}$ ,  $Zn_i$ s etc are inevitable<sup>3,30</sup> about which we will discuss in the context of PL. Furthermore, by given the core (ZnO)-shell (GO) structured it is logical to expect an increase in the interplanar spacing of graphene or stress related effects on ZnO. However, no angular shifts for either (002) of GO or (100), (002) and (101) of ZnO were suggested in Ref.<sup>3</sup> While, we have calculated lattice parameters for ZnO QDs and ZnO /GO QDs which are given in the following.  $a_{ZnO\ QDs} = 3.235$ ,  $c_{ZnO\ QDs} = 5.186$  Å and  $a_{ZnO/GO\ QDs} = 3.215$ ,  $c_{ZnO/GO\ QDs} = 5.147$  Å. It is apparent that the lattice parameters of ZnO/GO QDs are smaller than that of ZnO QDs. The quantitative changes (%) can be calculated by  $[a(c)_{ZnO\ QDs} - a(c)_{ZnO/GO\ QDs}]/a(c)_{ZnO\ QDs}$  yielding  $\sim 0.62$  and  $\sim 0.76\%$  for  $a$  and  $c$  values respectively.

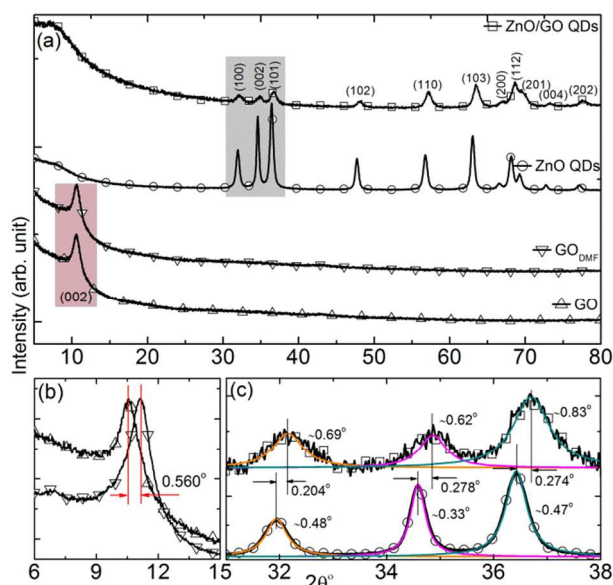


**Fig. 3.** XRD patterns from (a) GO,  $GO_{DMF}$ , ZnO QDs, ZnO/GO QDs (b) GO,  $GO_{DMF}$  (6-15°) and (c) ZnO QDs, ZnO/GO QDs (31-38°) with the fwhm values and angular shifts annotated.

The atomic percentages (at.%) of the constituting elements from the each of the samples are tabulated in Figure 4a. Core-level XP spectra of O1s, C1s and Zn2p are shown in Figure 4b-d, while the area ratios of O1s and C1s are annotated. We discuss the C to O ratios latter. From Figure 4a ZnO QDs depict slightly higher oxygen content than zinc which might be due to the chemisorbed oxygen ( $O_{Ch}$ ) on the surface and  $V_{OS}$ .<sup>31,32</sup> In the case of ZnO/GO QDs the higher oxygen content can be from oxygenous functional groups of GO. However, we expect some contribution from  $O_{Ch}$ . Carbon from ZnO QDs and might have arose from atmospheric contamination, glue of the copper tape that we have used to load the samples into the analysis chamber, in addition to a fraction of residual starting materials. The same is true for ZnO/GO QDs, however additional contribution to the carbon comes from graphene. The energetic location of O1s from ZnO ( $O_{ZnO}$ ) is consistent with the literature ( $\sim 530.4$  eV, Figure 4b).<sup>17,31,33</sup>  $O_{Ch}$  appeared at 532.2 eV indicated incorporation of  $-OH$ ,  $-CO$ , adsorbed  $H_2O$  and/or  $O_2$  or  $O^-$  and  $O^{2-}$  ions<sup>17,33-35</sup> essentially occupying the  $V_{OS}$  which play a critical role in the emission properties and related applications.<sup>16,17,31,32</sup>

C1s spectra from GO,  $GO_{DMF}$ , ZnO/GO QDs suggested three oxygenous functional groups (C-O, C=O and O-C=O) with varying fraction apart from C=C (Figure 4c).<sup>33</sup> GO has depicted a ratio of C:O::0.82:1.44. During the oxidation process oxygenous functional groups are implanted on the basal plane and edges of the graphene sheets.<sup>7</sup> This covalent functionalization increases the interplanar distance as evidenced in the XRD. Analysis on GO and  $GO_{DMF}$  suggest that total O at.% decreased apart from some N incorporation presumably due to DMF treatment ( $GO_{DMF}$  C:O::1.38:1). It is also noted that a fraction of conversion of C=O to C-O may be originated from the protonation of carbonyls by  $-CH_3$  groups of DMF. On the other hand, for the increase of O-C=O, the presence of  $-OH$  ions was attributed. It is convincing as we did not use anhydrous solvent in addition to the hydrophilic nature of GO. Further ZnO/GO QDs have shown C:O::1.93:1 which is higher than that of  $GO_{DMF}$ . In the former case, due to the presence of  $Zn^{+2}$  ions some of the functional groups are shielded in contrast to  $GO_{DMF}$ . This shielding hindered the access to DMF leaving the functional groups unreduced. We will see that in the context of Raman with slightly increased interplanar spacing of GO due to the presence of ZnO QDs. The changes in the density of oxygenous functional groups are consistent with the observation in XRD. In Ref.<sup>3</sup> the analysis of O1s core-level spectrum suggested fractional contributions are about 22% (C-O); 54% (O-C=O) and 22% (C=O) (Figure S3-2, supplementary information of Ref.<sup>3</sup>). Due to the presence of DMF during the synthesis, C=O will be converted into C-O, apart from an increase in the O-C=O group. The presence of O-C=O groups in such high concentrations requires a full consideration

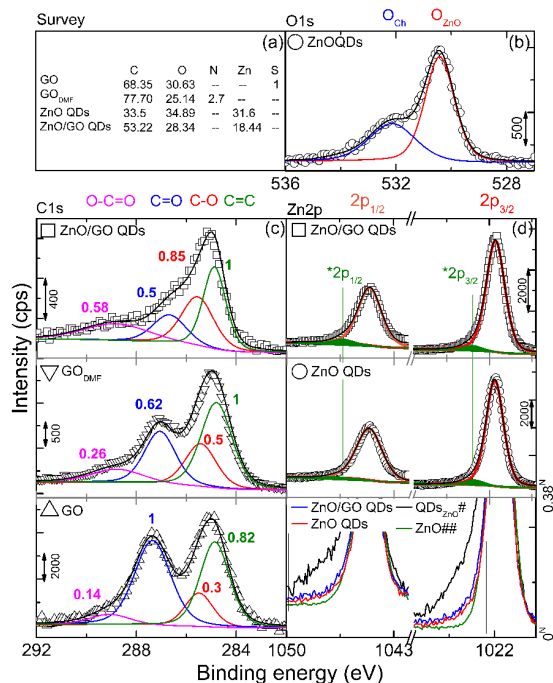


**Fig. 4.** (a) Atomic %s, (b) O1s from ZnO QDs, (c) C1s from GO, GO<sub>DMF</sub>, ZnO/GO QDs and (d) Zn2p from ZnO QDs, ZnO/GO QDs, normalized plot compares with ZnO. Data taken from the given references #<sup>17</sup>, ##<sup>32</sup>. N normalized intensity scale.

in the context of optoelectronic properties which is not the case in Ref.<sup>3</sup> On the other hand the presence of C=O functional groups (Figure S3-2 (b), supplementary information of Ref.<sup>3</sup>) is not discussed<sup>3</sup> in the context of interaction with Zn<sup>2+</sup> in addition to its electron-trapping capability under excited state.<sup>4,36</sup> These groups do interact with Zn<sup>2+</sup> however, depending on the strength of the acidic nature.<sup>6</sup> The integral effect of all the existing oxygenous functional groups forms the QDs during the reaction.

Moving onto Figure 4d, Zn2p from ZnO QDs and ZnO/GO QDs were compared with literature.<sup>17,32</sup> For both the cases the doublet peak positions (Zn2p<sub>3/2</sub> and Zn2p<sub>1/2</sub> at ~1021.5 and ~1044.5 eV, respectively) and fwhm values match with the literature.<sup>17,31-33</sup> Apart from the Zn2p doublet two additional peaks (\*2p<sub>3/2</sub> and \*2p<sub>1/2</sub> shaded in green) are observed at higher binding energies for both the samples. These peaks are attributed to the presence of Zn<sub>s</sub>,<sup>17,32,33</sup> however, such deconvolution of ionic state should be corroborated appropriately. In line with this we have co-plotted the normalized spectra from QDs<sub>ZnO</sub># and ZnO## where the former consists of significant density of Zn<sub>s</sub> while the latter is a well developed grainy coating (data taken from given reference #<sup>17</sup> and ##<sup>32</sup>). Zn<sub>s</sub> are seen to occur in the presence inhomogeneous distribution of functional groups on the surface of the substrate<sup>17</sup> apart from Zn rich environments.<sup>20</sup> Interestingly, although at present the substrate is not the same as that of Ref.<sup>17</sup> the interaction between the functional groups and Zn<sup>2+</sup> appears to play a crucial role. Please consult ref.<sup>17</sup> for further details on synthesis and structure. The high energy tails of the Zn2p<sub>3/2</sub> and Zn2p<sub>1/2</sub> need to be inspected for shoulder like structure (boxed region on Figure 4d, bottom). In the case of QDs<sub>ZnO</sub># the shoulder at higher energy is quite clear. It is notable that the intensity of the shoulder decreases ZnO/GO QDs, ZnO QDs and ZnO## in that order. As we can see in the case of well

developed and virtually defect free (Zn-related) surface there is no shoulder. This analysis essentially suggests the presence of Zn<sub>s</sub> in ZnO/GO QDs and ZnO QDs of varying density which will be revealed through specific energy lines in the PL.

The Raman spectrum of GO is characterized by two main components, D and G bands. D-band: edges, defects or the breakdown of translational symmetry. G-band: first order scattering of E<sub>2g</sub> phonon of sp<sup>2</sup> carbon atoms.<sup>37</sup> Raman response from GO, GO<sub>DMF</sub> and ZnO/GO QDs are shown Figure 5. Spectrum from GO has shown two signature peaks at ~1355 and ~1598 cm<sup>-1</sup> corresponding to D and G bands, respectively. Interestingly the peak at ~1355 cm<sup>-1</sup> did not show any significant spectral shift for the two modifications while the latter is shifted to ~1580 and ~1590 cm<sup>-1</sup> upon DMF treatment and ZnO QDs growth process, respectively. It might be the case that the distance between the graphene sheets is decreased<sup>37</sup> (lowered density of oxygenous functional groups) upon DMF treatment. However, due to the ZnO QDs and/or sustained degree of oxidation (interacting Zn<sup>2+</sup>) the distance between the sheets is increased again and the G-band is recovered to an extent. However, this is not seen explicitly in the XRD due to relatively lower signal to noise ratio. It is not denied that the DMF treatment might increase the already established defects such as changing bond lengths, angle and disorder at atomic scale which eventually soften the phonon modes.<sup>37</sup> If this is the case then G-band may not retrieve to 1590 cm<sup>-1</sup> for ZnO/GO QDs. Hence the softening of phonons is attributed to the decreased distance between the sheets than any other attribution. Note that the shift is not due to adsorbed DMF as no overlap of the peaks (\* on Figure 5) is seen within the detection limits. From Raman studies, it is also clear that the graphene in

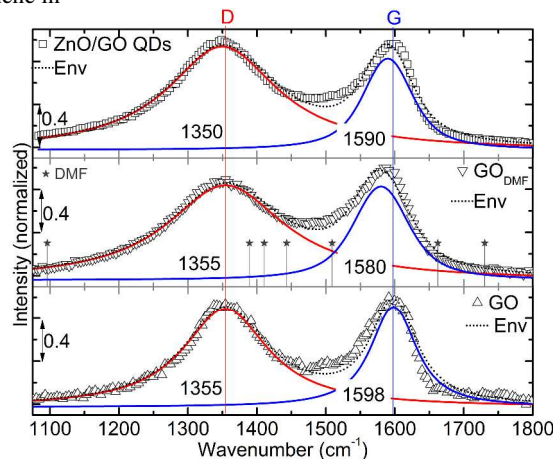


**Fig. 5.** Raman spectra from GO, GO<sub>DMF</sub> and ZnO/GO QDs with peak deconvolution. Modes from pure DMF are denoted with \*. The spectral locations were annotated in cm<sup>-1</sup>.

ZnO/GO QDs is not identical to that of GO<sub>DMF</sub> in all aspects as expected due to the growth of ZnO QDs. Such changes in the degree of oxidation can be seen in the context of fluorescence properties.<sup>2,5</sup> Son et al.<sup>3</sup> noticed splitting of G-band for ZnO/GO QDs (G<sup>-</sup> and G<sup>+</sup> at 1566.6 and 1592.7 cm<sup>-1</sup> respectively) and attributed to uniaxial strain on graphene (monolayer) under a first order approximation.<sup>38</sup> In contrast to Ref.<sup>3</sup> uniaxially bent graphene layer<sup>38</sup> has shown G<sup>-</sup> and G<sup>+</sup> at ~1563 and ~1576 cm<sup>-1</sup> (approximated from the plot). i.e. G band splits and shifts to lower frequencies whereas G<sup>+</sup> has shown a significant blue shift of ~17 cm<sup>-1</sup>. This shift cannot be attributed to the 'assumption' of uniaxial strain<sup>3</sup> however biaxial strain is certainly closer to ZnO/GO QDs case due to the spherical structure of QD. Nevertheless, in the case of biaxial strain no splitting is

observed<sup>39-41</sup> apart from the red-shifted G-band.<sup>39</sup> Although biaxial strain better represents the core-shell configuration in Ref.<sup>3</sup>, the blue shift of  $G^+$  might have arisen majorly due to ZnO. Despite, the presence of strain is not excluded in the current scenario. Contextually note that in the case of electron doping G band blue shifts.<sup>42</sup> On the other hand, the presence of 3 at.% of N might cause significant change in the electron density of GO thus the position of G band. Nevertheless, a deeper understanding of the influence of ZnO QDs under strain on the Raman modes of graphene is warranted.

We have analyzed the emission properties of GO,  $GO_{DMF}$ , ZnO QDs and ZnO/GO QDs and plotted them in Figure 6a-d respectively. L1 and L2 on part (b) indicate the spectral overlap of the emission peaks and hence not to be attributed to  $Zn_i$ s and ex- $Zn_i$ s. In Ref.<sup>3</sup> the earlier mentioned lines, L1 and L2 are attributed to  $GO_{epoxy}$  and  $E_v$  transitions (intersystem crossings<sup>3,15</sup>, see Figure 6e ( $E_c$ -conduction band and  $E_F$ -Fermi level). However, in XPS the presence of  $Zn_i$ s and possible formation of ex- $Zn_i$ s is evidenced<sup>3,30</sup> while their emission is schematized in Figure 6f. In what follows is the discussion on each of the samples in relation to the present attribution and the origin of green emission. In general, the intrinsic lattice defects and surface states are predominant in QDs.<sup>24</sup> In the case of ZnO it is known that visible emission occurs from the surface<sup>18,21,22</sup> in which case, the extremely high surface area to volume ratio of QDs plays a critical role. To begin with, the fluorescence from GO is under severe discussion.<sup>2,5</sup> Peak annotated with R is due to Raman scattering which occurred at  $\sim 378$  nm ( $\sim 350$  nm illumination) for both GO and  $GO_{DMF}$ . An overview of recent literature on the emission from GO and reduced-GO is given in Ref.<sup>2</sup> Emission from GO is excitation dependent (see ref. 86–88 in Ref.<sup>2</sup>) and attributed to the various possible transitions from the minimum of conduction band to localized states in the valance band. Basically the fluorescence from GO is explained based on two arguments. 1. The presence of oxygenous functional groups on the basal plane. In this case the emission occurs from zigzag sites of GO where their ground state is in a triplet state similar to carbene, 2. quantum confinement of  $sp^2$  domains ( $\pi$ -electrons) and  $e/h$  recombination therein. In this case, the local band gap depends on the size of the cluster. For  $GO_{DMF}$  the reaction with DMF incorporated nitrogen (XPS and Raman) which can influence the emission characteristics via doping the GO. Going into specifics, for GO (Figure 6a) two peaks are noted in the blue region at  $\sim 416$  and  $\sim 452$  nm (apart from two more components) which were slightly blue shifted to  $\sim 409$  and  $\sim 434$  nm respectively for  $GO_{DMF}$  case (Figure 6b).<sup>2</sup> Based on the literature and the available explanation<sup>3</sup> we believe that these two blue emissions may be due to confinement of  $sp^2$  domains. The blue shift of blue emission can be due to increased confinement after DMF treatment. After DMF treatment the other two peaks at 520 and 597 nm have almost distinguished. This can be due to the over-all decrease in the degree of oxidation,  $d$  value ( $d_{GO} > d_{GO_{DMF}}$ ) and conversion of some functional groups.<sup>2,5</sup> Hence these higher wavelength peaks may be attributed to the oxygenous functional groups. Interestingly the blue emission peaks from  $GO_{DMF}$  ( $\sim 409$  and  $\sim 434$  nm) spectrally overlap with that of L1:(LUMO + 2) $GO_{epoxy} \rightarrow E_v$  at 406 nm and L2:(LUMO) $GO_{epoxy} \rightarrow E_v$  at 436 nm from Ref.<sup>3</sup> We wish to point out that the emission bands could have been due to the  $GO_{DMF}$  juxtaposing with the proposed intersystem crossing. This spectral overlap is crucial to address and rule-out the possibility of emission from  $GO_{DMF}$ . The PL/optical emission spectra from ZnO QDs and ZnO/GO QDs are shown in Figure 6c and d respectively. The band gap of the each sample is calculated as the sum of exciton emission and its binding

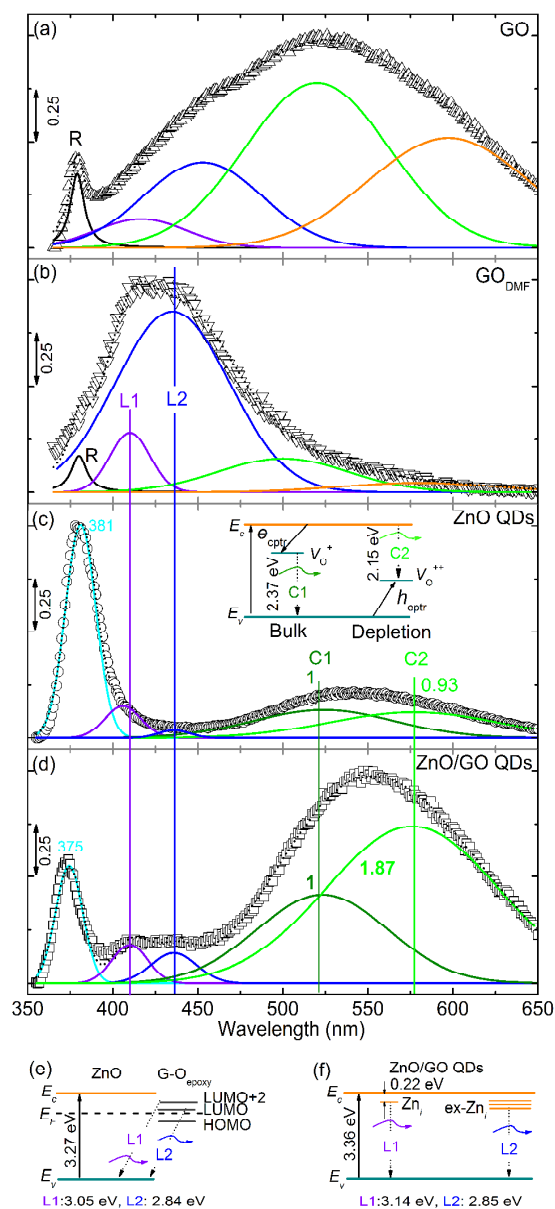


**Fig. 6.** Fluorescence from (a) GO, (b)  $GO_{DMF}$ , PL/optical emission from (c) ZnO QDs, (d) ZnO/GO QDs, (e) schematic of the two emission lines redrawn after Son et al.<sup>3</sup> and (f) ZnO/GO QDs with defect levels  $Zn_i$  and ex- $Zn_i$  states, insert of (c) depicts the schematic of the green emission from ZnO. Area ratio is indicated with reference to that of 524 nm (C1) peak in respective sample.  $E_c$ ,  $E_v$  are conduction and valance bands respectively, while  $e_{cptr}$  and  $h_{cptr}$  are electron and hole capture processes respectively and  $E_F$  is Fermi level. L1 and L2 on part (b) only indicate the spectral overlap of the emission peaks and hence not to be attributed to  $Zn_i$ s and ex- $Zn_i$ s.

energy (60 meV) yielding 3.31 eV and 3.36 eV for ZnO QDs and ZnO/GO QDs, respectively (Figure 6f). The slight increase in the band gap can be attributed to quantum confinement effect, in line with the earlier discussed growth mechanism. The 2D growth of ZnO on the surface of GO enhanced the confinement from pristine QDs. The green-emission from ZnO is attributed to  $V_O^*$  consisting of two components. Specifically, C1: 524 nm (2.37 eV):  $V_O^* \rightarrow E_v$ , and C2: 577 nm (2.15 eV)  $E_c \rightarrow V_O^{++}$ , which take place in bulk and

depletion regions, respectively (inset of Figure 6c).<sup>16,18,19,21-23,43</sup>  $V_{O}^{+}$  states either capture an electron ( $e$ ) or hole ( $h$ ) from  $E_c$  or  $E_v$ , respectively. i.e.  $V_{O}^{+} + e \rightarrow V_{O}^{*}$  and  $V_{O}^{+} + h \rightarrow V_{O}^{++}$ . Furthermore, the area ratios of C1 to C2 across the two ZnO containing samples are considered which reflect the emission from the corresponding regions. The ratios are  $(C1:C2)_{ZnO\ QDs}:1:0.93$ ;  $(C1:C2)_{ZnO/GO\ QDs}:1:1.87$ . Explicitly in ZnO/GO QDs sample there is almost two fold variation in the area of the C2.<sup>16,19</sup> The enhanced C2 emission is convincing because of the fact that the GO<sup>6,10,11</sup> and ZnO<sup>16,19</sup> are  $p$ - (depending on the degree of oxidation) and intrinsic  $n$ -type materials, respectively. The volume of the depletion region is increased due to the presence of GO which enhances the C2 as we observed here. Note that in the ZnO QDs case the occupancies of  $V_{OS}$  form the depletion region. To further comment on this, the observed changes in the relative emissions of C1 and C2 may not be an interfacial quenching, which requires a transfer of photoexcited electrons from  $E_c$  of ZnO to  $E_F$  of graphene.<sup>44</sup> In this case the whole emission is expected to decrease. However, we don't completely rule out such a possibility if the GO is sufficiently metallic within the interface.

In the blue region of ZnO QDs two peaks are seen, 405 nm (L1) and (435) L2 while the latter depicted relatively low intensity. Zn2p core-level spectrum evidenced the presence of  $Zn_{i,s}$  in smaller density from ZnO QDs which is reflected in the PL. The above two lines are attributed to  $Zn_{i,s}$  and ex- $Zn_{i,s}$ , respectively (L1:  $Zn_i \rightarrow E_v$  and L2: ex- $Zn_i \rightarrow E_v$ )<sup>20</sup> and consistent with the literature.<sup>17,20,23</sup>  $Zn_{i,s}$  are about 0.22 eV below the  $E_c$ ,<sup>45</sup> while ex- $Zn_{i,s}$  are ~0.5 eV below  $E_c$ .<sup>20</sup> Under suitable illumination, electrons are excited to the  $E_c$ , which are then non-radiatively transit into  $Zn_{i,s}$  or ex- $Zn_{i,s}$ . Also electron transfer can take place from  $Zn_{i,s}$  to ex- $Zn_i$  and subsequently to  $E_v$ . These localized electrons recombine with free holes in the  $E_v$  leading to violet or blue emission.<sup>20</sup> The presence of GO prior to the formation of ZnO QDs has significant influence on its growth, where the  $Zn^{2+}$  ions are anchored to the oxygenous functional groups of GO. Also, during the growth GO-sheets wrap the QD either partially or completely (Figure 2 and Figure 2 of Ref.<sup>3</sup>). Although the GO sheets are flexible XRD results suggested spatial or physical restriction that is imposed on interacting- $Zn^{2+}$  ions which may cause lattice defects such as  $Zn_{i,s}$  on the surface.<sup>17,20</sup> Zn2p core-level spectra suggested slightly higher density of  $Zn_{i,s}$  in ZnO/GO QDs than that of ZnO QDs, which is clearly reflected in the emission. These  $Zn_{i,s}$  form ex- $Zn_i$  states<sup>20</sup> as we can see the prominent difference in L2 across the two samples. For ZnO QDs, L1 due to  $Zn_{i,s}$  should occur at 3.09 eV which is at 3.05 eV with reference to the band gap (abbreviated as 'L1-ZnO QDs/ $Zn_{i,s}$ : 3.09/3.05 eV'). Similarly L2-ZnO QDs/ex- $Zn_{i,s}$ : 2.8/2.86 eV, L1-ZnO/GO QDs/ $Zn_{i,s}$ : 3.14/3.03 eV and L2-ZnO QDs/ex- $Zn_{i,s}$ : 2.85/2.85 eV. A small disagreement between the emitted and expected lines is due the differences in the band gap, error involved in deconvolution procedure. Especially for ZnO/GO QDs it can be a combination with the fluorescence from GO. The presence of C = O functional groups may decrease the quantum efficiency of the ZnO/GO QDs by trapping the electrons under excited state.<sup>4,36</sup> The consequences of trapping will be explicit in the context of optoelectronic properties as noted earlier.<sup>4</sup> However, the efficiency trapping of photoexcited electrons is determined by its recombination dynamics and physical accessibility. i.e. the functional group must be fast enough to trap the electron before the recombination. It is also notable that the recombination dynamics are influenced by electron and hole mobilities against the intrinsic electric field due to the depletion layer. By given these the complete quenching of emission from ZnO due to C=O groups can be an ideal scenario. Furthermore, since emission is seen from ZnO/GO QDs, it is believed that the density of C=O was not high enough to quench the emission completely, where

the DMF treatment has converted the C=O groups in to C-O groups. Earlier it is mentioned that the ZnO QDs are not fully covered by GO. However, the fraction of which can be very low that it would not undermine the discussion. The uncovered ZnO would not suppress the emission from ZnO/GO QDs rather we observe an integral effect from both uncovered ZnO and ZnO/GO QDs depending on their relative fractions. In the mixed case the peak area corresponding to the intrinsic defects cannot be simply attributed to individual constituents (when the exact fraction is unknown). Nevertheless, the defect emission wouldn't change its spectral position and should be evident. The existence of uncovered ZnO QDs in large fractions is unlikely, for instance XRD of ZnO/GO QDs did not depict any peaks with shoulders, which exhibit the contribution from uncovered ZnO QDs. Furthermore, XRD evidenced significant stress on the ZnO lattice in ZnO/GO QDs. *Viz* the quantitative changes (%) were ~0.62 and ~0.76% for  $a$  and  $c$  values respectively. Xu et al.<sup>26</sup> suggested piezotronic effect on the PL of ZnO nanowires (NWs) where excitonic emission red-shifts with increasing stress. Essentially the piezoelectric field ( $\pm\phi$ ) redistributes the photoexcited carriers along with modified band structure of a bent ZnO NW causing a red-shift. The following parameters determine the presence of piezotronic effect. (a)  $|\phi|$  critically depends on the doping density ( $N_D$ ) while the latter can partially or totally screen the  $\phi$ .<sup>28</sup> (b) For  $W \ll d_{NW}$  the red-shift is independent of the  $d_{NW}$ . When  $W \approx d_{NW}$  the red-shift is dependent on the  $d_{NW}$ , which decreases with decreasing  $d_{NW}$ .<sup>26</sup> (c) single crystals depicted piezotronic<sup>26</sup> and piezoelectric response<sup>27,28</sup> (when bent along  $c$ -axis) and highly  $c$ -axis oriented thinfilms<sup>46</sup> exhibited piezoelectric response. In the present case we did not observe any piezotronic effect in ZnO/GO QDs despite of the strain due the following reasons corresponding to the above factors. (a') For ZnO,  $N_D$  is determined by point defects such as  $Zn_{i,s}$  and  $V_{OS}$ .<sup>47</sup> ZnO QDs consists of intrinsic defects ( $Zn_{i,s}$  and  $V_{OS}$ ) as explicitly evidenced in the PL (Fig. 6c). The same is true for ZnO/GO QDs (Fig. 6d) where the defects are more pronounced and hence the relatively higher  $N_D$  screening the  $\phi$ . (b') For QDs,  $W$  is most probably as thick as the diameter. Moreover,  $W$  would be relatively higher for ZnO/GO QDs case due to the  $p$ -natured GO (seen from the area ratios of green emission). Since  $W \approx d_{NW}$  any shift is governed by the size of the QDs. From Fig.5c of Ref.<sup>26</sup> as the diameter of the NW decreases the red-shift of free exciton emission decreases, essentially approaching  $W \approx d_{NW}$ . (c') ZnO QDs and ZnO/GO QDs are polycrystalline without any preferential orientation. Piezotronic response is realized when a compressive strain is applied along  $c$ -axis of NW<sup>26,28</sup> while  $a$  is allowed to modulate most probably increases its value. Significantly, here  $c$  and  $a$  were subjected to compressive strain. It may be the case that the developed  $\phi$  along one axis is compensated by the other axis. Furthermore, the  $\phi$  may be compensated by GO, where there is a net supply of electrons from GO despite of it being a  $p$ -type material.<sup>6,10,11</sup>

## Conclusions

The ionic interaction between  $Zn^{2+}$  ions and the oxygenous functional groups influences the growth of ZnO QDs, where the lattice of the latter is slightly compressed. Due to the earlier mentioned interaction XPS evidenced  $Zn_{i,s}$  where their density in ZnO/GO QDs is higher than that of pristine counterpart. Analysis on Raman spectra suggested deeper investigation to understand the influence of ZnO on GO. We do acknowledge the fact that the analysis of optical emission from complex systems is not a simple arithmetic sum of two or more components, rather it involves various combinatory factors. Nevertheless, we provide direct conclusions with spectroscopic evidence on two vital issues regarding

the mechanism of luminescence from ZnO/GO composite. (i) L1 and L2 have two alternative possibilities, *viz*  $Zn_i \rightarrow E_v$  and  $ex-Zn_i \rightarrow E_v$  respectively and (ii) these two emissions might be from GO. The interaction between GO and  $Zn^{2+}$  is the basis for the existence of  $Zn_s$  as evidenced in the XPS and subsequently in PL. Also the presence of  $Zn_s$  can perhaps explain the emission from the light emitting diode structure.<sup>3</sup> Under biased conditions the charge carriers may be injected from GO into the  $Zn_i$  or  $ex-Zn_i$  states which eventually recombine with free holes in the  $E_v$  emitting light of matching wavelength. (B) Luminescence centered at 550 nm is attributed to  $V_{OS}$  with two components and a width of about 0.3 eV each in contrast to 0.8 eV shown in Ref.<sup>3</sup>. In the ZnO/GO QDs the emission from depletion region is enhanced twice due to the presence of GO. The absence of piezotronic effect in ZnO/GO QDs despite of a significant strain is attributed to the increased  $N_D$ ,  $W \approx$  diameter of the QDs, compressive strain along  $c$  and  $a$  axes and to the presence of GO.

## Acknowledgements

S.V. thanks The Scientific & Technological Research Council of Turkey (TUBITAK) (TUBITAK-BIDEB 2221-Fellowships for Visiting Scientists and Scientists on Sabbatical) for the postdoctoral fellowship. A. C. thanks to TUBITAK (Project no. 113Y348) for the postdoctoral fellowship. TU acknowledges The Turkish Academy of Sciences–Outstanding Young Scientists Award Program (TUBA-GEBIP).

## Notes and references

<sup>a</sup> UNAM-National Nanotechnology Research Centre, Bilkent University, Ankara, 06800, Turkey.

<sup>b</sup> Institute of Materials Science & Nanotechnology, Bilkent University, Ankara, 06800, Turkey.

SV: svempati01@qub.ac.uk

1. A. M. Dimiev and J. M. Tour, *ACS Nano*, 2014, **8**, 3060–3068.
2. S. Vempati and T. Uyar, *Phys. Chem. Chem. Phys.*, 2014, **16**, 21183–21203.
3. D. I. Son, B. W. Kwon, D. H. Park, W. S. Seo, Y. Yi, B. Angadi, C. L. Lee and W. K. Choi, *Nat. Nanotechnol.*, 2012, **7**, 465–471.
4. S. Vempati, S. Ozcan and T. Uyar, *Appl. Phys. Lett.*, 2015, **106**, 051106.
5. K. P. Loh, Q. L. Bao, G. Eda and M. Chhowalla, *Nat. Chem.*, 2010, **2**, 1015–1024.
6. S. Vempati, A. Celebioglu and T. Uyar, *J. Mater. Chem. C*, 2015, **2**, 8585–8592.
7. D. C. Marcano, D. V. Kosynkin, J. M. Berlin, A. Sinitskii, Z. Sun, A. Slesarev, L. B. Alemany, W. Lu and J. M. Tour, *ACS Nano*, 2010, **4**, 4806–4814.
8. B. Yao, C. Li, J. Ma and G. Shi, *Phys. Chem. Chem. Phys.*, 2015, DOI: 10.1039/C5CP02853A.
9. P. Shao, J. Tian, B. Liu, W. Shi, S. Gao, Y. Song, M. Ling and F. Cui, *Nanoscale*, 2015, DOI: 10.1039/C5NR03042K.
10. R. J. W. E. Lahaye, H. K. Jeong, C. Y. Park and Y. H. Lee, *Phys. Rev. B*, 2009, **79**, 125435.
11. M. Jin, H.-K. Jeong, W. J. Yu, D. J. Bae, B. R. Kang and Y. H. Lee, *J. Phys. D: Appl. Phys.*, 2009, **42**, 135109.
12. S. Mondal, U. Rana and S. Malik, *Chem. Commun.*, 2015, DOI: 10.1039/C5CC03981A.
13. Q. Luo, Y. Zhang, C. Liu, J. Li, N. Wang and H. Lin, *J. Mater. Chem. A*, 2015, DOI: 10.1039/C5TA02710A.
14. Y. Wang, Y. Li, W. Qi and Y. Song, *Chem. Commun.*, 2015, **51**, 11022–11025.
15. S. S. Bao, Z. Hua, X. Y. Wang, Y. Zhou, C. F. Zhang, W. G. Tu, Z. G. Zou and M. Xiao, *Opt. Express*, 2012, **20**, 28801–28807.
16. S. Vempati, S. Chirakkara, J. Mitra, P. Dawson, K. K. Nanda and S. B. Krupanidhi, *Appl. Phys. Lett.*, 2012, **100**, 162104.
17. F. Kayaci, S. Vempati, I. Donmez, N. Biyikli and T. Uyar, *Nanoscale*, 2014, **6**, 10224–10234.
18. K. Vanheusden, C. H. Seager, W. L. Warren, D. R. Tallant and J. A. Voigt, *Appl. Phys. Lett.*, 1996, **68**, 403.
19. J. D. Ye, S. L. Gu, F. Qin, S. M. Zhu, S. M. Liu, X. Zhou, W. Liu, L. Q. Hu, R. Zhang, Y. Shi and Y. D. Zheng, *Appl. Phys. A: Mater. Sci. Process.*, 2005, **81**, 759.
20. H. Zeng, G. Duan, Y. Li, S. Yang, X. Xu and W. Cai, *Adv. Funct. Mater.*, 2010, **20**, 516–572.
21. A. v. Dijken, E. A. Meulenkaamp, D. Vanmaekelbergh and A. Meijerink, *J. Phys. Chem. B*, 2000, **104**, 1715.
22. K. Vanheusden, W. L. Warren, C. H. Seager, D. R. Tallant, J. A. Voigt and B. E. Gnade, *J. Appl. Phys.*, 1996, **79**, 7983.
23. S. Vempati, J. Mitra and P. Dawson, *Nanoscale Res. Lett.*, 2012, **7**, 470.
24. S. Vempati, Y. Ertas and T. Uyar, *J. Phys. Chem. C*, 2013, **117**, 21609–21618.
25. *X-ray penetration depth (1/e of intensity,  $\delta$ ) =  $1/(\xi\rho)$ , where  $\rho$ -density ( $g/cm^3$ ) and  $\xi$ -mass attenuation coefficient ( $cm^2/g$ ).  $\xi$  was taken from [\[http://physics.nist.gov/PhysRefData/XrayMassCoeef/tab3.html\]](http://physics.nist.gov/PhysRefData/XrayMassCoeef/tab3.html).  $\xi_{Zn}=58.75$ ,  $\xi_O=11.63$ ,  $\xi_{ZnO}=\xi_{Zn} + \xi_O$ ,  $\rho_{ZnO}=5.61$ ;  $\xi_{graphite}=4.57$ ,  $\rho_{graphite}=2.27$ ; yielding  $\delta_{ZnO} \sim 25 \mu m$  and  $\delta_{graphite} \sim 960 \mu m$ .*
26. S. Xu, W. Guo, S. Du, M. M. T. Loy and N. Wang, *Nano. Lett.*, 2012, **12**, 5802–5807.
27. B. Wei, K. Zheng, Y. Ji, Y. Zhang, Z. Zhang and X. Han, *Nano. Lett.*, 2012, **12**, 4595–4599.
28. Z. L. Wang, *J. Phys. Chem. Lett.*, 2010, **1**, 1388–1393.
29. H. Luth, *Solid Surfaces, Interfaces and Thin Films*, Springer, ISBN 978-3-642-13591-0, e-ISBN 978-3-642-13592-7, DOI 10.1007/978-3-642-13592-7, Fifth Edition edn., 2010.
30. S. Niyogi, E. Bekyarova, M. E. Itkis, J. L. McWilliams, M. A. Hamon and R. C. Haddon, *J. Am. Chem. Soc.*, 2006, **128**, 7720–7721.
31. F. Kayaci, S. Vempati, C.O.-Akgun, I. Donmez, N. Biyikli and T. Uyar, *Appl. Catal. B.*, 2015, **176**, 646–653.
32. F. Kayaci, S. Vempati, C.O.-Akgun, I. Donmez, N. Biyikli and T. Uyar, *Nanoscale*, 2014, **6**, 5735–5745.
33. A. V. Naumkin, A.K.-Vass, S. W. Gaarenstroom and C. J. Powell, *Journal*, 2012, **NIST Standard Reference Database 20, Version 4.1**.
34. M. Chen, X. Wang, Y. Yu, Z. Pei, X. Bai, C. Sun, R. Huang and L. Wen, *Appl. Surf. Sci.*, 2000, **158**, 134–140.
35. A. Stănoiu, C. E. Simion and S. Somănescu, *Sens. Actu. B: Chem.*, 2013, **186**, 687–694.
36. H. Chang, Z. Sun, Q. Yuan, F. Ding, X. Tao, F. Yan and Z. Zheng, *Adv. Mater.*, 2010, **22**, 4872.
37. A. C. Ferrari, *Solid State Commun.*, 2007, **143**, 47–57.



38. T. M. G. Mohiuddin, A. Lombardo, R. R. Nair, A. Bonetti, G. Savini, R. Jalil, N. Bonini, D. M. Basko, C. Galiotis, N. Marzari, K. S. Novoselov, A. K. Geim and A. C. Ferrari, *Phys. Rev. B*, 2009, **79**, 205433.
39. J. Zabel, R. R. Nair, A. Ott, T. Georgiou, A. K. Geim, K. S. Novoselov and C. Casiraghi, *Nano. Lett.*, 2011, **12**, 617-621.
40. F. Ding, H. Ji, Y. Chen, A. Herklotz, K. Dorr, Y. Mei, A. Rastelli and O. G. Schmidt, *Nano. Lett.*, 2010, **10**, 3453.
41. C. Metzger, S. Remi, M. Liu, S. V. Kusminskiy, A. H. N. Castro, A. K. Swan and B. B. Goldberg, *Nano. Lett.*, 2010, **10**, 6.
42. S. Pisana, M. Lazzeri, C. Casiraghi, K. S. Novoselov, A. K. Geim, A. C. Ferrari and F. Mauri, *Nat. Mater.*, 2007, **6**, 198.
43. M. Ghosh and A. K. Raychaudhuri, *Nanotechnology*, 2008, **19**, 445704.
44.  *$E_F$  equilibration takes place when the materials are brought into contact.*
45. C. H. Ahn, Y. Y. Kim, D. C. Kim, S. K. Mohanta and H. K. Cho, *J. Appl. Phys.*, 2009, **105**, 013502.
46. I. K. Bdikin, J. Gracio, R. Ayouchi, R. Schwarz and A. L. Kholkin, *Nanotechnology*, 2010, **21**, 235703.
47. Y. Gao and Z. L. Wang, *Nano. Lett.*, 2009, **9**, 1103-1110.